Bioactive Materials 44 (2025) 516–530

Contents lists available at ScienceDirect

Bioactive Materials

journal homepage: www.keaipublishing.com/en/journals/bioactive-materials

Conductive polyphenol microneedles coupled with electroacupuncture to accelerate wound healing and alleviate depressive-like behaviors in diabetes

Yue Hou [a,1], Xiaochuan Guo [b,1], Jinhui Ran [a], Xiong Lu [a,*], Chaoming Xie [a,**]

[a] Institute of Biomedical Engineering, College of Medicine, Southwest Jiaotong University, Chengdu, Sichuan, 610031, China
[b] Department of Rehabilitation Medicine, Affiliated Hospital of Southwest Jiaotong University, The Third People's Hospital of Chengdu, Chengdu, Sichuan, 610031, China

ARTICLE INFO

Keywords:
Diabetic wound healing
Inflammatory modulation
Hydrogel microneedle
Electroacupuncture
Depression

ABSTRACT

Inflammation and depression are serious complications of diabetes that interact to form a feedback loop and may hinder diabetic wound healing. They share a common pathophysiological basis of abnormal interactions between diabetic wounds and the brain. Here, we propose a strategy combining electroacupuncture (EA) stimulation of the Dazhui acupoint (GV14) with polyphenol-mediated conductive hydrogel microneedles to promote diabetic wound healing and alleviate depression through local wound–brain interactions. The conductive microneedles comprised methacrylated gelatin, dopamine (DA), DA-modified poly(3,4-ethylenedioxythiophene), and *Lycium barbarum* polysaccharide. EA at GV14 activated the vagus–adrenal axis to inhibit systemic inflammation while DA coupled electrical signals for long-term inhibition of local wound inflammation. EA at GV14 was also found to elevate 5-hydroxytryptamine levels in rats with diabetic wounds, consequently mitigating depressive-like behaviors. Additionally, the polyphenol-mediated conductive hydrogel microneedles, and coupled with EA stimulation promoted healing of wound tissue and peripheral nerves. This strategy regulated both local and systemic inflammation while alleviating depressive-like behaviors in diabetic rats, providing a new clinical perspective for the treatment of diabetes-related and emotional disorders.

1. Introduction

Diabetes usually leads to chronic, non-healing wounds that can progress to diabetic foot ulcers (DFU), posing a risk of lower limb amputation. In addition to causing a significant physical burden, diabetes also predisposes patients to depression [1,2]. The inflammatory response triggered by a high-glucose microenvironment is pivotal in the onset of depression [3–5], a common and debilitating comorbidity in diabetic wounds. It reduces the chances of remission and treatment adherence [6,7], while elevating the risk of disability and mortality in affected patients, thus perpetuating a detrimental circuit in disease progression and potentially worsening the wound healing process. Oral or injectable medicines that decrease advanced glycation end products closely associated with reactive oxygen species (ROS) are commonly administered to control the systemic inflammation [8]. Current local treatment approaches for DFU entail debriding necrotic tissue, administering antibiotics to manage local infections, and applying wound dressings [9]. However, these approaches overlook the impact of depression and its negative impact on wound healing. Strategies to simultaneously target diabetic wounds and modulate depression have not yet been reported.

Electroacupuncture (EA) is a systemic regulatory technique that involves the application of electrical stimulation to specific points on the body known as acupoints, activating neural networks and thereby systematically regulating systemic inflammation [10,11]. It is commonly used to treat chronic diseases and alleviate depression without the use of medicines and their potential side effects [12,13]. Recently, EA at the Zusanli acupoint (ST36) was reported to activate prokineticin receptor 2-expressing sensory neurons, which transmit signals to the vagus–adrenal axis to control systemic inflammation [14]. Furthermore,

Peer review under responsibility of KeAi Communications Co., Ltd.
* Corresponding author.
** Corresponding author.
E-mail addresses: luxiong_2004@163.com (X. Lu), xie@swjtu.edu.cn (C. Xie).
[1] These authors contributed equally to this work.

https://doi.org/10.1016/j.bioactmat.2024.11.001
Received 5 July 2024; Received in revised form 1 November 2024; Accepted 1 November 2024

EA offers exogenous electrical stimulation to enhance peripheral nerve repair [15,16]. EA-mediated anti-inflammatory effects are highly specific to certain acupoints. For example, stimulation of the Dazhui acupoint (GV14) has been shown to effectively regulate inflammation and immunity, and has been utilized as a treatment for spinal cord injury and fever [17,18]. EA can restore synaptic plasticity by regulating monoamine neurotransmitter expression in the hippocampus, thereby relieving depressive symptoms [19]. However, EA alone faces challenges in directing and promptly managing the local inflammatory microenvironment of wounds.

Hydrogel microneedles represent a modality for wound local regulation exerted via aiding the promotion of wound healing. As a drug

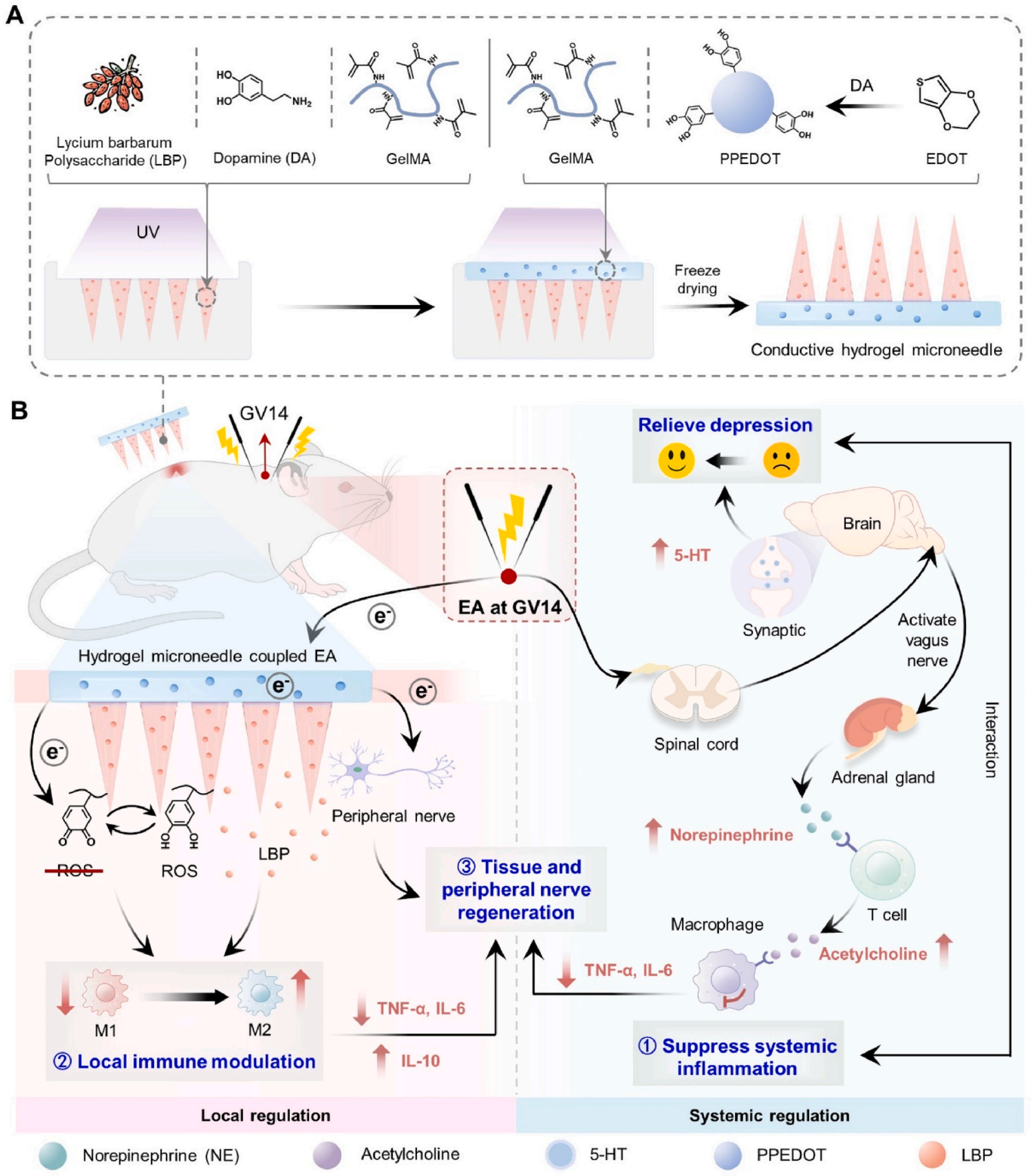

Fig. 1. Schematic diagram of hydrogel microneedle preparation and the wound repair mechanism. (A) Preparation of hydrogel microneedles. (B) Synergistic mechanism of hydrogel microneedles combined with EA at GV14 to treat and enhance repair of skin wounds in diabetic rats.

delivery system, hydrogel microneedles exhibit efficient penetration of the stratum corneum while avoiding nerve tissue [20], and thus have potential for modulating local inflammation and immune responses in diabetic wounds with minimal tissue damage and pain. Additionally, the integration of electrical signals can simulate natural electrophysiological properties, influencing cellular behavior and facilitating tissue repair [21]. However, non-conductive types of microneedles cannot be used to couple EA-induced electric signals. The incorporation of conductive nanoparticles (e.g. carbon nanotubes, graphene, pyrrole, 3, 4-ethylenedioxythiophene) into microneedles has been employed to confer conductive properties. Nevertheless, many conductive nanoparticles have a low dispersibility in water and are not compatible with hydrogel systems. Notably, endowing a microneedle with conductivity to transmit electrical signals only represents a physical coupling, not a functional coupling.

Natural extracts have gained significant attention for their multiple biological activities and minimal side effects in diabetic wound repair. LBP, a natural extract from wolfberry, improves the diabetic wound microenvironment and promotes tissue regeneration by enhancing immune function, reducing oxidative stress, and stimulating cell proliferation [22]. Natural polyphenols (e.g. dopamine [DA], tannins, epigallocatechin gallate, gallic acid) have been shown to exhibit antioxidant activity with effective free radical scavenging, as well as anti-inflammatory and wound healing properties exerted by intracellular signaling pathways that modulate immune responses [23]. Previous research found that polyphenols not only accept electrons to promote phenol-quinone redox balance and achieve long-lasting anti--inflammatory and anti-oxidative effects, but also serve as surface coatings to enhance the dispersion of conductive nanoparticles [24–26]. Therefore, the construction of conductive hydrogel microneedles that regulate the local microenvironment of diabetic wounds through polyphenol chemistry coupled with EA can be applied to effectively co-manage diabetic wounds and depression.

In this study, we proposed a combined approach using conductive hydrogel microneedles and EA at GV14 for the synergistic regulation of local and systemic inflammation, alleviation of diabetes-induced depression, and promotion of diabetic wound healing. The hydrogel microneedles were primarily composed of gelatin-methacryloyl (GelMA), polydopamine-modified poly(3,4-ethylenedioxythiophene) nanoparticles (PPEDOT), DA, and *Lycium barbarum* polysaccharide (LBP) (Fig. 1A). EA at GV14 suppressed systemic inflammation via the vagus–adrenal axis and also increased 5-hydroxytryptamine (5-HT) levels, alleviating depressive symptoms in rats with diabetic wounds. PPEDOT provided conductivity to the microneedles, coupling EA for modulation of the wound microenvironment. DA provided potent and long-term anti-inflammatory and antioxidant properties under external electrical stimulation provided by EA. Furthermore, polyphenol-mediated microneedles released LBP and synergized with electroacupuncture to promote regeneration of wound tissues and peripheral nerves.

2. Experimental section

2.1. Preparation of dopamine-modified poly3,4-ethylenedioxythiophene (PPEDOT)

The dissolution of 0.05 g of DA in 20 mL of deionized water was to be carried out simultaneously with the dissolution of 2 g of APS in 25 mL of deionized water. Subsequently, 600 μL of EDOT was to be added to 45 mL of absolute ethanol. The aforementioned DA aqueous solution was to be stirred for 5 min in order to dissolve this mixture. The APS solution was combined with the mixed solution and continuously stirred in an ice-water bath for 24 h to achieve complete polymerization of the EDOT and DA monomers, resulting in a color change to blue-black. The solution was then centrifuged with deionized water (8000 r/min, 5 min) to eliminate impurities until the supernatant became colorless and transparent. Finally, PPEDOT nanoparticles were obtained, dispersed in deionized water, and stored at 4 °C for subsequent use. PEDOT nanoparticles, prepared without the addition of DA, were also produced using the same method.

2.2. Preparation of the DA-LBP-PPEDOT-GelMA hydrogel microneedle

The DA-LBP-PPEDOT-GelMA hydrogel microneedle was prepared via the following steps. Typically, GelMA (0.75 g) was dissolved in deionized water (5 mL) to form GelMA solution at 60 °C. Then the DA (0.01 g), LBP (0.02 g), PEGDA (75 μL) and I2959 (0.075 g) were added into the GelMA solution to form precursor solution A. Simultaneously, the PPEDOT (0.05 g/ml), PEGDA (75 μL) and I2959 (0.075 g) were added into the GelMA solution to form precursor solution B. Following this, solution A was introduced into the microneedle mold and evacuated to fill the mold tip, then cross-linked under UV light irradiation to form the needle tip. Subsequently, solution B was applied to the microneedle mold to generate a backing layer, which was likewise cross-linked under UV irradiation. Ultimately, the freeze-drying process yielded hydrogel microneedles with sufficient hardness to penetrate the epidermis.

For comparison, we prepared hydrogel microneedles with different compositions. Table S1 shows the specific components of the hydrogel microneedles.

2.3. In vitro cytocompatibility and cell affinity of the hydrogel microneedle

L929 mouse fibroblasts, acquired from the Kunming Cell Bank (Kunming, China), were employed to assess the cytocompatibility of the hydrogel microneedle. The L929 fibroblasts were cultured in high-glucose Dulbecco's modified Eagle's medium (DMEM, Gibco), supplemented with 10 % FBS and 1 % penicillin-streptomycin, within a humidified incubator maintained at 37 °C with 5 % CO_2. L929 cells (4×10^4 cells/well) were seeded onto each hydrogel (GelMA, DA-GelMA, DA-LBP-GelMA, and DA-LBP-PPEDOT-GelMA) in 48-well plates. The dimension of hydrogel samples was 10 mm in diameter and 1 mm in thickness. The hydrogels underwent purification through repeated immersion in PBS solution and 75 % ethanol for 5 days to eliminate unreacted monomers and ensure sterilization. Following 1 and 3 days of cultivation, the cells on the hydrogels were stained with calcein AM (Beyotime, China) and propidium iodide (Beyotime, China), then examined using a confocal laser scanning microscope (CLSM, LSM880, Carl Zeiss, Germany).

Cell viability was quantified through a 3(4,5-dimethylthiazol-2-yl)-2,5-diphenyltetrazolium bromide (MTT, Biosharp, China) assay. MTT solution (0.5 mg/mL, 400 μL/well) was introduced to the plate at 37 °C. After 4 h, 400 μL of dimethyl sulfoxide (DMSO) replaced the MTT solution, and the plates were incubated in a concussion incubator for 15 min. Finally, the absorbance (OD) of the solution was measured at 570 nm using a microplate reader (WD-2102A; LIUYI Technologies, Beijing, China).

2.4. Cell culture under electrical stimulation

L929 cells (4×10^4 cells/well) were seeded onto each hydrogel (GelMA and PPEDOT-GelMA) in 48-well plates. Starting from the second day post-cell inoculation, cells underwent electrical stimulation with a density wave at 2/100 Hz for 20 min daily, facilitated by an acupoint nerve stimulator (HANS-200A, Lianchuang, China). Cell viability was assessed using the MTT assay at 1 and 3 days following electrical stimulation. Five days after electrical stimulation, the cell culture medium was collected, and the levels of type I collagen (Col-I) and α-smooth muscle actin (α-SMA) were measured using ELISA kits.

RSC96 rat Schwann cells (Procell, China) were employed to assess the impact of conductive hydrogel on neural cell under electrical

stimulation. The RSC96 Schwann cells were cultured in high-glucose Dulbecco's modified Eagle's medium, supplemented with 10 % FBS and 1 % penicillin-streptomycin, within a humidified incubator maintained at 37 °C with 5 % CO_2. RSC96 cells (4×10^4 cells/well) were seeded onto each hydrogel (GelMA, PPEDOT-GelMA) in 48-well plates. Starting from the second day post-cell inoculation, cells underwent electrical stimulation with a density wave at 2/100 Hz for 20 min daily, facilitated by an acupoint nerve stimulator (HANS-200A, Lianchuang, China). Following 2 days of electrical stimulation, cells on the samples were fixed using a 4 % paraformaldehyde solution and prepared for staining. DAPI (Solarbio, China) was employed to stain the nucleus (blue), while fluorescein isothiocyanate-labeled phalloidin (P5282, Sigma) was utilized to stain F-actin (red). The cellular morphology was subsequently observed using CLSM.

2.5. In vitro ROS scavenging ability of the hydrogel microneedle

RAW 264.7 cells (3×10^5 cells per well) were seeded onto GelMA, DA-GelMA, DA-LBP-GelMA, and DA-LBP-PPEDOT-GelMA hydrogels in 24-well plates and cultured in DMEM supplemented with 10 % (v/v) FBS. Following 12 h of cell culture, cells were subjected to stimulation with 100 μM of H_2O_2 (500 μL per well) after removing the culture medium for 2 h and washing with PBS three times. Subsequently, a DCFH-DA (10×10^{-3} M, 500 μL per well) probe molecule was added. After 20 min, the levels of reactive oxygen species (ROS) were assessed using CLSM. The group without H_2O_2 stimulation served as the control.

2.6. Polarization of macrophages

RAW 264.7 macrophages (5×10^4 cells per well) were seeded onto various hydrogels in 24-well plates. Macrophages were polarized into M1 phenotypes through treatment with 100-ng/mL LPS cultured with different hydrogels. For CD163 and inducible nitric oxide synthase (iNOS) staining, RAW 264.7 cells were fixed in 4 % (w/v) paraformaldehyde, and the macrophages were incubated with primary antibodies. Donkey anti-rabbit antibody, Alexa Fluor 488 (1:800, A-21206, Invitrogen, USA), and donkey anti-rabbit antibody, Alexa Fluor 555 (1:800, A-31572, Invitrogen, USA) served as secondary antibodies. Finally, cell nuclei were labeled with DAPI (ab1041139, Abcam, USA). The cellular morphology was observed using CLSM.

2.7. Quantitative real-time PCR (qPCR) of RAW264.7

RAW 264.7 cells (1×10^5 cells per well) were cultured on GelMA, DA-GelMA, and DA-LBP-GelMA hydrogel surfaces in 48-well plates for 2 days. Macrophages were polarized to the M1 phenotype through treatment with 100 ng/mL LPS and cultured with various hydrogels. Following the extraction of total RNA, it was reverse transcribed into complementary DNA. The real-time fluorescence quantitative PCR system (ABI, StepOnePlus) was employed to detect the gene expression of TNF-α and IL-10. The group inoculated in well plates and treated with LPS served as the control group. Table S3 presents the primer sequences used for the tested genes.

2.8. Model establishing

A full-thickness skin wound model in type II diabetic rats was employed to assess the in vivo performance of distinct groups of hydrogel microneedles. Male SD rats (8–10 weeks old) underwent an 8-h fasting period and received intravenous injections of streptozotocin (55 mg/kg). After one week, the fasting blood glucose level surpassed 16.5 mM, indicating successful modeling. SD rats were procured from Chengdu Dossy Experimental Animals Co., Ltd. (Chengdu, China). Diabetic rats were initially anesthetized with 3 % sodium pentobarbital (1 mL/kg). Following the removal of hair on the dorsal skin, four full-thickness wounds, each with a diameter of 10 mm, were carefully generated.

2.9. Suppressing systemic inflammation

This experiment was conducted on a diabetic rat with a full-thickness skin defect. The experiment was divided into three groups: (1) A group that utilized an acupoint nerve stimulator to electrically stimulate the Dazhui point (GV14); (2) A group that employed an acupoint nerve stimulator to electrically stimulate the wound area; (3) A control group that did not receive any treatment. During the initial three days following the creation of a full-thickness skin defect, electrical stimulation was administered once daily for 20 min per session, followed by subsequent sessions every other day. On the seventh day, 30 min after the end of EA stimulation, blood was collected from the hearts of the rats and centrifuged to obtain serum. The levels of norepinephrine, IL-6, TNF-α and IL-1β were then evaluated using ELISA kits.

2.10. Inhibiting local inflammation

The experiment was bifurcated into two segments: non-electrical stimulation and electrical stimulation. In the non-electrical stimulation segment, hydrogel microneedles including PPEDOT-GelMA, DA-PPEDOT-GelMA, DA-LBP-GelMA, and DA-LBP-PPEDOT-GelMA were randomly administered to four wounds on the dorsal area of rats, whereas wounds in the Blank group were left untreated with any material. In the electrical stimulation segment, rats were randomly assigned to receive either DA-LBP-Gel or DA-LBP-PPEDOT-GelMA hydrogel microneedles applied to four wounds on the backs of rats. The Blank group did not receive any materials post-surgery. Electroacupuncture stimulation was administered once daily for three days. On the fourth day, skin tissues from all groups were collected for immunofluorescence staining of IL-6 and TNF-α. Images were captured using a confocal laser scanning microscope (CLSM; Eclipse C1, Nikon, Japan). Relative fluorescence area was analyzed using ImageJ (version 1.8.0_172).

2.11. Behavioral tests

The experiment was divided into four groups: (1) Application of DA-LBP-PPEDOT- GelMA hydrogel microneedles to the skin defect with concurrent electroacupuncture stimulation of GV14 (Wound (EA + microneedle)); (2) Electroacupuncture stimulation of GV14 (Wound (EA)); (3) Creation of wounds without any treatment (Wound); (4) No wounds were induced, serving as the Control. During the initial three days following the creation of a full-thickness skin defect, electrical stimulation was administered once daily for 20 min per session, followed by subsequent sessions every other day. Behavioral testing was conducted on the eighth day.

Open field test: The test was conducted within a black plastic square box ($100 \times 100 \times 50$ cm^3) without a lid. The rat was placed in the central area and allowed to explore for 5 min. Behaviors, such as movement trajectories and the proportion of time spent actively in the central area, were recorded and assessed.

Tail suspension test: The rat was suspended by its tail for a duration of 6 min. The final 4 min of immobility, following a 2-min habituation period, were recorded. To minimize the impact of visual and auditory stimuli during the experiment, rats were suspended individually.

2.12. Diabetic wound healing

The experiment was bifurcated into two segments: non-electrical stimulation and electrical stimulation. In the non-electrical stimulation segment, hydrogel microneedles including PPEDOT-GelMA, DA-PPEDOT-GelMA, DA-LBP-GelMA, and DA-LBP-PPEDOT-GelMA were randomly administered to four wounds on the dorsal area of rats, whereas wounds in the Blank group were left untreated with any ma-

terial. In the electrical stimulation segment, rats were randomly assigned to receive either DA-LBP-GelMA or DA-LBP-PPEDOT-GelMA hydrogel microneedles applied to four wounds on the backs of rats. The Blank group did not receive any materials post-surgery. Electroacupuncture stimulation was administered every other day post-operation, and photographs were taken at specified time intervals (days 0, 7, 14, and 21) to document the wound's condition. The percentage of wound closure was calculated as follows:

$$\text{Wound closure percentage} = (A_0 - A_t) / A_0$$

where A_0 represents the initial wound area and A_t denotes the wound area at each time point post-surgery

On the 21st day, wound tissue was obtained for H&E staining and immunofluorescence staining of peripheral nerves (PGP-9.5 and MBP). Images were captured using a confocal laser scanning microscope (CLSM; Eclipse C1, Nikon, Japan). Relative fluorescence area was analyzed using ImageJ (version 1.8.0_172)

2.13. RNA-seq and data analysis

Three interventions were administered to diabetic rats with full-thickness skin defects: (1) Electroacupuncture stimulation of GV14 coupled with the application of DA-LBP-PPEDOT-GelMA hydrogel microneedles at the wound site (DA-LBP-PPEDOT-GelMA(EA)); (2) Electroacupuncture stimulation of GV14 coupled with the application of DA-LBP-GelMA hydrogel microneedles at the wound site (DA-LBP-GelMA(EA)); (3) Application of DA-LBP-PPEDOT-GelMA hydrogel microneedles at the wound site (DA-LBP-PPEDOT-GelMA). Electroacupuncture stimulation was conducted daily for the initial 3 days post-surgery, followed by every other day thereafter. On day 8, skin tissue samples were collected, and the RNA's total quantity and integrity were assessed using the Bioanalyzer 2100 System's RNA Nano 6000 Assay Kit (Agilent Technologies, CA, USA). RNA sequencing libraries were constructed and sequenced using Illumina NovaSeq 6000.

2.14. Quantitative real-time PCR (qPCR) of wound skin tissue from diabetic rats

Wound skin tissues were collected from the three groups of diabetic rats subjected to different treatments, as detailed in section 2.13. Following the extraction of total RNA, it was reverse transcribed into complementary DNA. The real-time fluorescence quantitative PCR system (ABI, Step One Plus) was employed to detect the gene expression of P38MAPK, PI3K, AKT and FOXP3. Table S4 presents the primer sequences used for the tested genes.

2.15. Statistical analysis

SPSS software was used to assess the statistical significance of all comparison studies in this work. In the statistical analysis for comparison between multiple samples, one-way analysis of variance (ANOVA) followed by Tukey's multiple comparison test were conducted with thresholds of $^*P \leq 0.05$, $^{**}P \leq 0.01$, and $^{***}P \leq 0.001$.

3. Results

3.1. Design strategy

The hydrogel microneedles consist of GelMA, PPEDOT, DA, and LBP. GelMA-based microneedles face limitations in conductivity, anti-inflammatory, antioxidant, and immunomodulatory properties, reducing their biomedical efficacy. GelMA is non-conductive, hindering its use in electrical stimulation applications, and integrating conductive materials without compromising mechanical integrity is challenging. It also lacks inherent anti-inflammatory, antioxidant, and immunomodulatory effects, requiring modifications or additives to improve therapeutic outcomes and immune responses. LBP and DA were incorporated into the microneedle tips to synergistically regulate local inflammation and promote wound healing. Subsequently, PPEDOT were added to the backing layer of the microneedles, providing outstanding electrical conductivity and facilitating long-term anti-inflammation and peripheral nerve repair in response to external electrical stimulation provided by EA. Simultaneously, EA at GV14 reduced blood inflammatory factors and increased 5-HT levels in rats with diabetic wounds, consequently relieving depression.

This design strategy achieved systemic regulation and local material response, achieving excellent therapeutic effects in the following ways (Fig. 1B). (1) Inhibition of systemic inflammation: Electrical signals transmitted from GV14 to the brain via the spinal cord. These signals stimulated the secretion of norepinephrine through the vagus–adrenal axis, facilitating the release of acetylcholine. Ultimately, this leads to downregulated secretion of inflammatory factors, inhibiting systemic inflammation. EA at GV14 also alleviated depression by increasing 5-HT levels; (2) Local immune regulation: EA promoted local immune regulation via the conversion of DA quinone to DA catechol through electron transfer, leading to continuous scavenging of free radicals, regulation of macrophage phenotypes, upregulation of anti-inflammatory factors, and downregulation of inflammatory factors; (3) Tissue and peripheral nerve regeneration: Conductive hydrogel microneedles coupled endogenous electrical signals and the response to exogenous electrical stimulation, thereby promoting the repair of wound tissue and epidermal nerves with LBP.

The interplay between local immune regulation and suppression of systemic inflammation offers a means to alleviate the impacts of inflammation on wound healing and depressive symptoms. Concurrently, local wound healing and amelioration of depressive symptoms also aid in lowering systemic inflammation levels, fostering a positive feedback loop of interactions between local wounds and the brain in diabetes. This virtuous circle could bolster patient recovery outcomes overall, facilitating the holistic restoration of both physical and psychological well-being.

3.2. Characterization of conductive nanoparticles and hydrogel microneedles

The binding capabilities of DA were central to the successful modification of PPEDOT. PPEDOT in a spherical form with a size of approximately 100 nm were observed (Fig. 2A). While PPEDOT exhibited excellent water dispersibility, PEDOT appeared to settle after 1 h (Fig. 2B). The polydispersity index (PDI) of PPEDOT was significantly lower than that of PEDOT, indicating that PDA modification effectively enhanced the dispersibility of the nanoparticles (Fig. S1). X-ray photoelectron spectroscopy (XPS) analysis offered conclusive evidence regarding the formation of PPEDOT, as illustrated in Fig. 2C. Drawing upon the chemical structure of DA, established intermediate species, and the proposed structure of polydopamine, the N1s region revealed three peaks attributed to primary ($R-NH_2$), secondary ($R-NH-R$), and tertiary/aromatic ($=N-R$) amine functional groups [27].

Conductive hydrogel microneedles were successfully fabricated through photoinitiation using GelMA, PPEDOT, DA, and LBP, with the back layer rendered conductive via PPEDOT (Fig. 2D). SEM images indicated that the microneedles were approximately 1100 μm in height with a base width of ~300 μm, and exhibited an ordered arrangement (Fig. 2E). Fourier transform infrared (FTIR) spectroscopy of GelMA and DA-GelMA hydrogels revealed a new peak at 875 cm^{-1} in DA-GelMA (Fig. S2), which confirms the presence of catechol units [28]. SEM image showed that the porous structure of the PPEDOT-GelMA hydrogel, with PPEDOT nanoparticles visibly distributed throughout the hydrogel (Fig. S3). The force-displacement curve of the microneedle array patch demonstrated that each needle possessed a mechanical strength of 0.09 N/needle prior to fracture (Fig. 2F), surpassing that

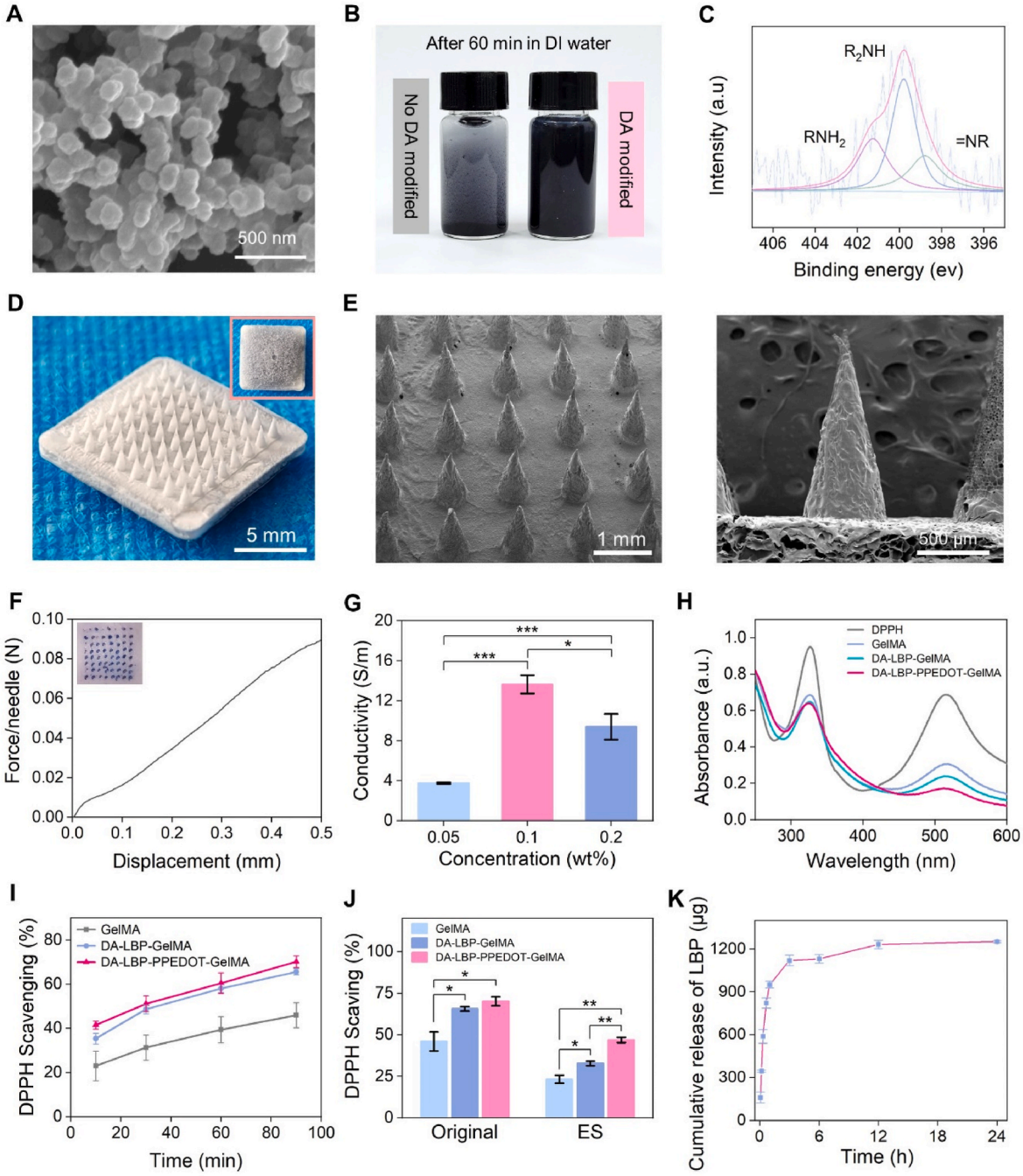

Fig. 2. Characterization of the physicochemical properties of conductive nanoparticles and hydrogel microneedles. (A) SEM image of PPEDOT. (B) Digital image of nanoparticle dispersion with and without DA modification. (C) XPS analysis of PPEDOT. (D) Digital image of the hydrogel microneedle array. (E) SEM images of the hydrogel microneedle. (F) Compression test of DA-LBP-PPEDOT-GelMA, with a digital image of punctured rat skin stained with trypan blue displayed in the upper left corner. (G) Electrical conductivity of hydrogel microneedles. (H) UV spectra of various hydrogel microneedles analyzed after a 90-min reaction with DPPH free radicals. (I) DPPH scavenging ability of hydrogel microneedles. (J) Restoration of DPPH free radical-scavenging efficiency through electrical stimulation post depletion of free radical-scavenging capacity (repeated scavenging of DPPH radicals). (K) LBP release from hydrogel microneedles.

required to penetrate the skin (0.06 N/needle) [29]. The mechanical properties of the hydrogel microneedles showed minimal variation across the different groups (GelMA, DA-GelMA, and DA-LBP-GelMA) (Fig. S4). Additionally, microneedle acupuncture sites in rat dorsal skin were stained with trypan blue, demonstrating correspondence with the microneedle array (Fig. 2F). The electrical conductivity of the microneedle base increased with increasing PPEDOT content up to 0.1 wt%, with a maximum electrical conductivity of 14 S/m. The conductivity initially increases but subsequently decreases as the PPEDOT content rises, due to aggregation of PPEDOT at high content (0.2 wt%) (Fig. 2G).

The conductive hydrogel microneedles demonstrated prolonged free radical scavenging capability. Results from the 2,2-diphenyl-1-picrylhydrazyl (DPPH) scavenging test revealed that DA-LBP-PPEDOT-GelMA exhibited the most significant decrease in absorption peak at 517 nm after 90 min (Fig. 2H), indicating high DPPH scavenging efficiency (Fig. 2I). Notably, upon application of external electrical stimulation, 46.86 % of the free radical-scavenging efficiency of DA-LBP-PPEDOT-GelMA was recovered after near exhaustion of its free radical-scavenging ability (Fig. 2J). In addition, DA-LBP-PPEDOT-GelMA

microneedles, whose free radical scavenging capacity had been nearly depleted, were applied in full-thickness skin defects in diabetic rats, followed by EA at GV14. After removal, the microneedles were tested for their DPPH scavenging activity, and the results showed that 25.13 % of their free radical scavenging efficiency was restored (Fig. S5). This was attributed to the excellent conductivity of DA-LBP-PPEDOT-GelMA conferred by PPEDOT, enabling it to facilitate the conversion of catechol-quinone through electron transfer in response to electrical stimulation. XPS analysis of PPEDOT after electrical stimulation revealed a decreasing trend in the peak corresponding to C=O bonds (Fig. S6 and Table S2).

Our hydrogel microneedles were capable of absorbing liquid and swelling without dissolving — a property that makes them advantageous for wound dressings and drug delivery. All hydrogel microneedles efficiently absorbed a significant amount of water within 30 min and achieved swelling equilibrium within 1 h (Fig. S7). DA-LBP-PPEDOT-GelMA also demonstrated superior sustained drug release ability, gradually releasing LBP over a 12 h interval (Fig. 2K and Fig. S8). Specifically, a near-linear rate of drug release was observed during the first 3 h, with gradual slowing and stabilization after 6 h. These findings demonstrated that our hydrogel microneedles exhibit efficient drug-release capability, gradually absorbing bodily fluids to create swelling that dispenses medication upon skin insertion.

3.3. Cytocompatibility, antioxidant, and immunomodulatory properties of hydrogel microneedles

To assess the cytocompatibility of our hydrogel microneedles, L929 fibroblasts were co-cultured with GelMA, PPEDOT-GelMA, DA-GelMA, and DA-LBP-GelMA hydrogels. The introduction of DA and LBP facilitated the proliferation of L929 cells compared with GelMA hydrogel, as demonstrated by fluorescence images of calcein AM staining after 1 and 3 days (Fig. 3A). These results were verified through quantitative analysis of cell proliferation using the 3-(4,5-dimethylthiazol-2-yl)-2,5-diphenyltetrazolium bromide (MTT) method, indicating ideal cytocompatibility (Fig. 3B).

The PPEDOT-GelMA layer of the double-layer hydrogel microneedle exhibits good electrical conductivity and thus serves as a conductive substrate to regulate cellular behavior and promote repair of peripheral nerves through transmission of electrical signals. To evaluate the impact of electrical stimulation on cell proliferation and differentiation, L929 cells were cultured on GelMA and PPEDOT-GelMA hydrogels, followed by electrical stimulation. Cell proliferation was evaluated using the MTT assay, and differentiation was assessed via ELISA kits for type I collagen (Col-I) and α-SMA. The results demonstrated that conductive hydrogels with electrical stimulation significantly promoted cell proliferation (Fig. S9). Furthermore, PPEDOT-GelMA with electrical stimulation notably upregulated Col-I and α-SMA levels, indicating enhanced cell differentiation (Fig. S10). To examine the impact of an external electric field collaborating with conductive hydrogel microneedles on cell behavior, RSC96 cells were cultivated on the surfaces of GelMA and PPEDOT-GelMA hydrogels under electrical stimulation (Fig. 3C and Fig. S11). To visualize cell morphology, phalloidin was used to stain RSC96 cells after 1 day of cultivation with GelMA and PPEDOT-GelMA hydrogels under electrical stimulation. As illustrated in Fig. 3D, RSC96 cells subjected to electrical stimulation displayed adhesion and spreading on PPEDOT-GelMA hydrogel that was superior to that on GelMA hydrogel. This difference was attributed to the enhanced electrical signal provided by PPEDOT. These results suggest that PPEDOT-GelMA hydrogels convey the external electrical signals necessary to stimulate cell spines, thereby regulating cell behavior.

Additionally, our hydrogel microneedles demonstrated antioxidative and immunomodulatory properties. DCFH-DA staining analysis of RAW 264.7 macrophages revealed that the hydrogel including DA and LBP had effective ROS scavenging ability. As shown in Fig. 3E, a robust fluorescence signal was visible in the cells stimulated with H_2O_2. The DCFH fluorescence intensity of cells under H_2O_2 stimulation started to decrease after treatment with DA-GelMA hydrogel, reaching a minimum after treatment with DA-LBP-GelMA hydrogel. These results demonstrated that the hydrogel microneedles have the ability to scavenge ROS.

The phenotype of macrophages cultured on the hydrogels was evaluated by measuring the expression levels of pro-inflammatory tumor necrosis factor (TNF)-α and anti-inflammatory interleukin (IL)-10 markers in the presence of lipopolysaccharide (LPS). As demonstrated in Fig. 3F, TNF-α expression levels were significantly lower in macrophages treated with DA-GelMA and DA-LBP-GelMA hydrogels than in macrophages treated with GelMA hydrogel or control (LPS treatment). Macrophages treated with DA-LBP-GelMA hydrogel exhibited the lowest TNF-α expression level. Furthermore, macrophages treated with DA-GelMA and DA-LBP-GelMA hydrogels demonstrated increased expression levels of IL-10, with the highest level in the DA-LBP-GelMA group (Fig. 3G). These findings indicated that both DA and LBP possess anti-inflammatory activity. Immunofluorescence staining results revealed a significantly lower level of inducible nitric oxide synthase (iNOS; a marker indicating M1 macrophage activation) in the DA-LBP-GelMA group compared with that in the other groups (Fig. 3H and I). Conversely, the DA-LBP-GelMA group exhibited the highest levels of CD163, a marker for M2 macrophage polarization, among the groups. These results demonstrated that DA possesses immunomodulatory capabilities that are amplified by the incorporation of LBP. Consequently, DA-LBP-GelMA hydrogel produced a synergistic effect that significantly reduced inflammatory cytokines and increased anti-inflammatory cytokines, thus altering polarization of macrophages from M1 to M2.

3.4. Repair of diabetic wounds and peripheral nerves

EA of GV14 in synergy with polyphenol-mediated conductive hydrogel microneedles effectively inhibited local and systemic inflammation and promoted repair of diabetic wounds and peripheral nerves (Fig. 4A). After anesthetizing SD rats and shaving their neck fur, acupuncture needles were inserted into the GV14 acupoint. An acupoint nerve stimulator was then connected to deliver electrical stimulation (Fig. S12). During the course of wound healing, digital images were captured to analyze the wound areas (Fig. 4B and C). PPEDOT-GelMA delivered enhanced wound closure compared with the Blank, primarily attributed to its superior conductivity, facilitating endogenous electric field repair and expediting wound healing. The addition of DA further augmented the wound-healing efficacy of DA-PPEDOT-GelMA, which was ascribed to its anti-inflammatory, antioxidant, and immunomodulatory properties. LBP, in conjunction with DA, additionally modulated local wound immunity, with DA-LBP-GelMA and DA-LBP-PPEDOT-GelMA exhibiting the most favorable wound healing rates under non-EA conditions. Upon synergistic EA at GV14, the wound healing rates of the Blank, DA-LBP-GelMA, and DA-LBP-PPEDOT-GelMA were further enhanced, with DA-LBP-PPEDOT-GelMA showing particularly noteworthy improvement. This enhancement was attributed to the response of the conductive hydrogel microneedles to EA, facilitating the conversion of catechol-quinone to achieve enduring anti-inflammatory effects. Healed wounds treated with the hydrogels were further evaluation through hematoxylin and eosin (H&E) staining (Fig. 4D). The gap lengths of granulation tissue were smaller in the wounds treated with DA-LBP-PPEDOT-GelMA (EA) (1 mm) than with non-conductive DA-LBP-GelMA (EA) (1.5 mm), and were significantly smaller than those in the other treatment groups (Fig. 4E). These findings demonstrated a significant improvement in the healing rate of diabetic wounds using DA-LBP-PPEDOT-GelMA (EA).

Conductive hydrogel microneedles used in EA have the ability to increase nerve repair in the vicinity of the wound. Protein gene product-9.5 (PGP-9.5) serves as a neuronal marker and myelin basic protein (MBP) is the principal component of the myelin sheath present in the

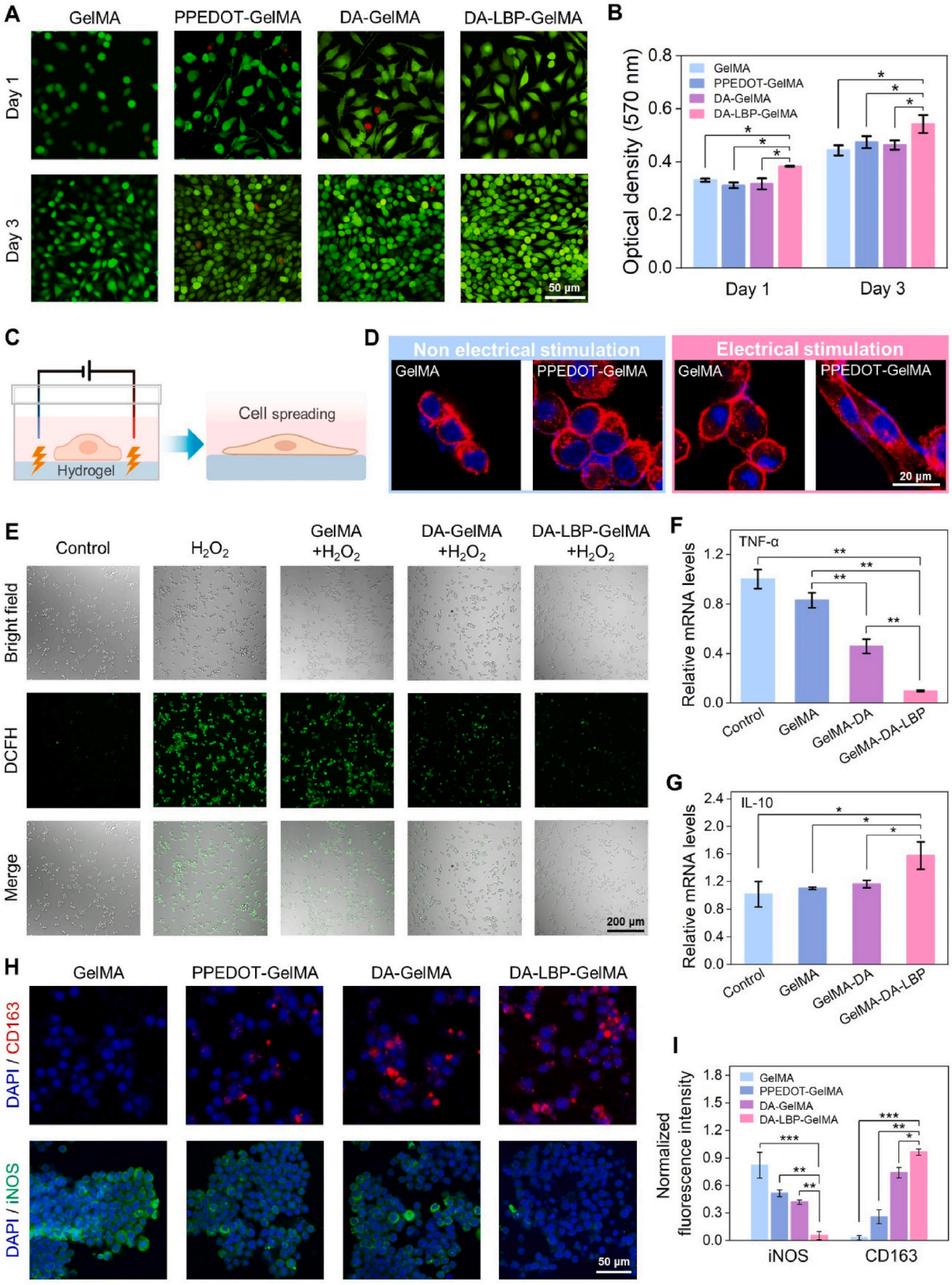

Fig. 3. Cytocompatibility and immunomodulatory properties of hydrogel microneedles. (A) Confocal laser scanning microscopy (CLSM) images of L929 cells cultured on different hydrogels for 1 or 3 days. Green color indicates living cells; red color indicates dead cells. (B) L929 cell proliferation on different hydrogels for 1 or 3 days. (C) Schematic diagram of electrical stimulation of cells. (D) CLSM images of Schwann cells with different treatments on day 3 cultured on different hydrogels. Blue color (DAPI) indicates cell nuclei; red color (phalloidin) indicates F-actin. (E) CLSM images of ROS in macrophages cultured on different hydrogels. (F, G) Expression levels of M1-related marker TNF-α (F) and M2-related marker IL-10 (G) in RAW 264.7 macrophages cultured on different hydrogels. (H) Fluorescence microscopy of iNOS and CD163 expression and nuclear staining of RAW 264.7 macrophages cultured on different hydrogels. (I) Quantification of the fluorescence intensities of iNOS and CD163.

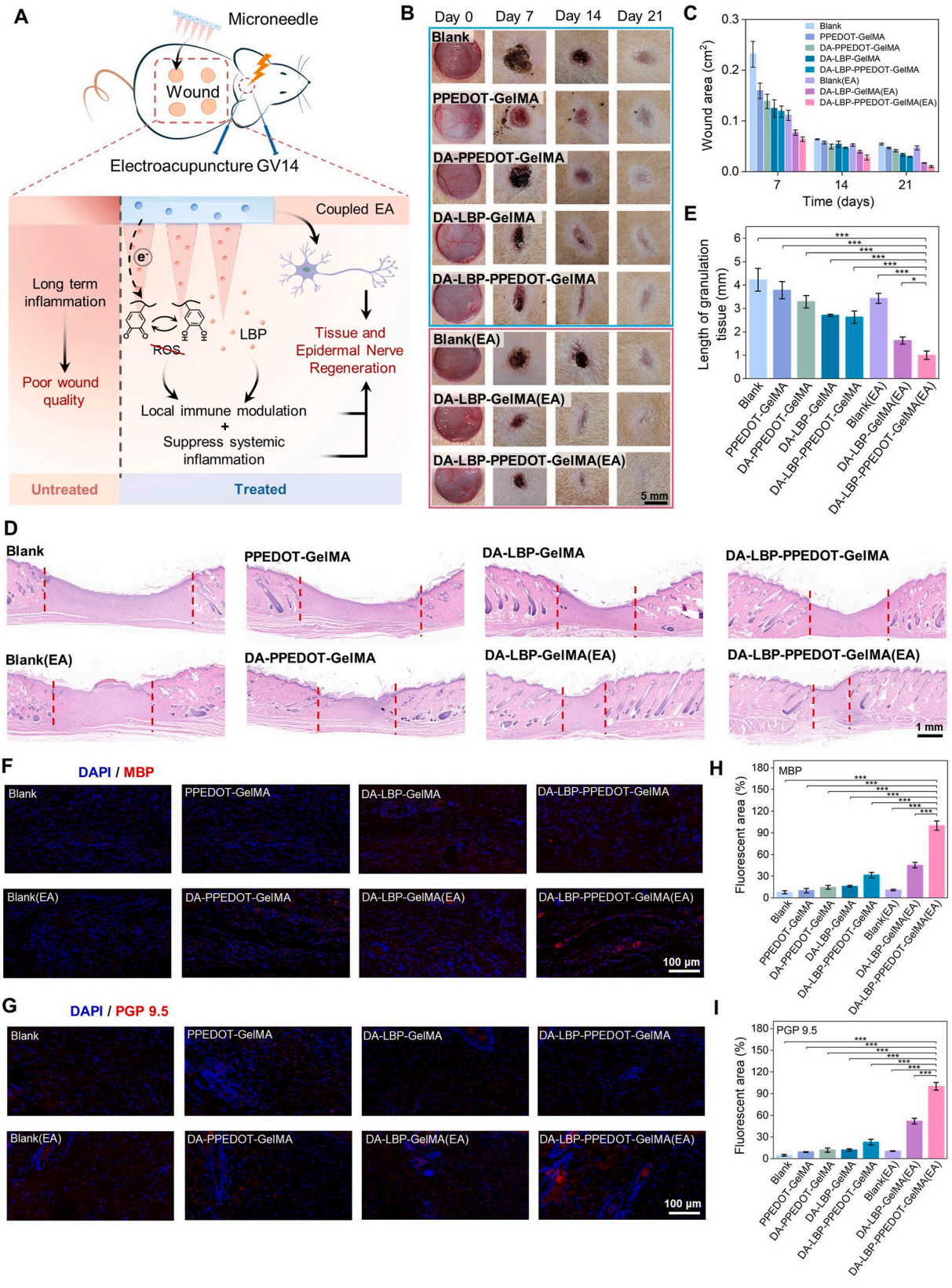

Fig. 4. Synergy between EA of GV14 and hydrogel microneedles in diabetic wound repair. (A) Schematic diagram of tissue and peripheral nerve repair. (B) Digital images of wounds treated with different hydrogels for the indicated time periods. (C) Size of the wound area in the different treatment groups at the indicated time points. (D) H&E staining of representative wound sections in each group after 21 days of healing. (E) Length of the granulation tissue gap in each group after 21 days. (F, G) Immunofluorescence staining images of MBP (F) and PGP-9.5 (G) in each group after 21 days. Blue color (DAPI) indicates nuclei; red color indicates MBP and PGP-9.5. (H, I) Relative fluorescent area of immunofluorescence images of MBP (H) and PGP-9.5 (I).

central nervous system and some neurons [30]. Immunofluorescence staining revealed prominent MBP red fluorescence in the dermis, with noticeable PGP-9.5 red fluorescence at the epidermal-dermal junction, of the DA-LBP-PPEDOT-GelMA (EA) group (Fig. 4F and G). These findings confirmed that this therapeutic approach fosters nerve regeneration in diabetic wounds. Further analysis indicated that EA at GV14 used as an adjunctive treatment significantly increased the fluorescent area compared with hydrogel microneedle treatment alone (Fig. 4H and I). This confirmed the role of GV14 stimulation in promoting nerve regeneration in diabetic wounds. However, the DA-LBP-PPEDOT-GelMA (EA) group displayed greater red fluorescence than the non-conductive DA-LBP-GelMA (EA) group, as did the DA-LBP-PPEDOT-GelMA group compared with the non-conductive DA-LBP-GelMA group. These findings implied that the integration of PPEDOT conferred the hydrogel microneedles with excellent electrical activity, aiding the modulation of endogenous electrical signals and the response to EA, ultimately promoting peripheral nerve regeneration. This process involves both peripheral nerve cells and non-neural cells. Cell experiments demonstrated that the exogenous electrical signals from the conductive hydrogel microneedles, combined with electroacupuncture, promote the adhesion and spreading of rat Schwann cells, which are crucial for normal nerve function and repair [31]. Furthermore, this treatment strategy effectively regulates the immune microenvironment by shifting macrophage polarization from M1 to the M2 phenotype, reducing inflammatory responses, and facilitating nerve repair and regeneration [32,33].

3.5. Alleviation of depression

Depressive behavior in rats with diabetic wounds was alleviated by the synergistic effect of polyphenol-mediated conductive hydrogel microneedles and EA at GV14. To assess the impact of various treatment approaches on depressive-like behavior in rats with diabetic wounds, the open field test and tail suspension test were employed. In the open field experiment (Fig. 5A–I), the rats in the diabetic wound (Wound) group exhibited minimal movement along the periphery of the open field, with almost no central movement route (Fig. 5A–II). In contrast, the Wound (EA) group treated with diabetic wounding + EA at GV14 demonstrated a notable increase in the central movement route. The Wound (EA + microneedle) group treated with DA-LBP-PPEDOT-GelMA synergistic EA displayed a further enhancement in the central motor route. Displaying a similar trend, the time spent by rats in the central area significantly increased following synergistic hydrogel microneedling of GV14 (Fig. 5A–III). In the tail suspension experiment (Fig. 5B), the immobility time of rats in the Wound group was significantly increased compared with that in the control group. Conversely, the immobility times in the Wound (EA) and Wound (EA + microneedle) groups were notably decreased.

Decreased 5-HT [34–36] and FOXP3 [37,38] levels are commonly observed in individuals with depression. Therefore, to evaluate the mechanism by which synergistic EA with DA-LBP-PPEDOT-GelMA microneedles modulated behavioral changes in diabetic rats, 5-HT and FOXP3 levels were measured in the different treatment groups (Fig. 5C and D). The levels of both 5-HT and FOXP3 were significantly increased in the Wound (EA) and Wound (EA + microneedle) groups compared with those in the Wound group, with a more substantial increase in the Wound (EA + microneedle) group that was nearly equivalent to that of the Control group. In summary, the utilization of polyphenol-mediated conductive hydrogel microneedles on diabetic wounds, coupled with concurrent EA of GV14, demonstrated superior efficacy in diabetic wound healing and depression alleviation.

3.6. Regulation of systemic and local inflammation

The benefits of conductive microneedle synergistic EA at GV14 were also attributed to the regulation of both local and systemic inflammation (Fig. 5E). To assess the impact of GV14 EA on inhibition of systemic inflammation, diabetic rats with a wound created on the back were divided into three experimental groups: EA(Wound) treated with EA around the wound, EA(GV14) treated with EA at GV14, and a control group without any further intervention. Serum norepinephrine levels measured after 7 days were highest in the EA(GV14) group (0.37 ± 0.01 ng/mL; Fig. 5F). Liver concentrations of acetylcholine were also highest in the EA(GV14) group (24.75 ± 0.30 ng/g; Fig. 5G). The serum concentrations of inflammatory factors IL-6 and TNF-α were both significantly reduced in the EA(GV14) group (Fig. 5H). These results demonstrated that EA of GV14 inhibited systemic inflammation.

Next, we further validated the localized anti-inflammatory impact of hydrogel microneedles and explored their synergistic anti-inflammatory effect in combination with EA at GV14. Immunofluorescence staining images (Fig. 5I and J) of the wound site after 3 days of treatment revealed that the fluorescent area in the DA-LBP-PPEDOT-GelMA group was significantly smaller than that in the Blank group, confirming the local anti-inflammatory effect of DA-LBP-PPEDOT-GelMA. In addition, the Blank (EA) group had a slightly reduced fluorescent area compared with the Blank group, indicating that EA at GV14 had an inhibitory effect on local inflammation at the wound site. Furthermore, the smallest fluorescent area was observed in the DA-LBP-PPEDOT-GelMA (EA) group, providing strong evidence of the synergistic anti-inflammatory effect of hydrogel microneedles combined with EA at GV14.

3.7. Potential pathways of the regulation of inflammation and depression

RNA sequencing was utilized to elucidate the synergistic mechanism between EA at GV14 and DA-LBP-PPEDOT-GelMA in promoting the repair of diabetic wounds. Comparison of gene expression in wound skin tissue under treatment with the various hydrogel microneedles, with and without EA, yielded numerous differences and 60 shared genes (Fig. 6A). Compared with DA-LBP-PPEDOT-GelMA, DA-LBP-PPEDOT-GelMA (EA) led to differential expression of 3286 genes (1413 upregulated and 1873 downregulated) (Fig. 6B). Compared with non-conductive DA-LBP-GelMA (EA) treatment, conductive DA-LBP-PPEDOT-GelMA (EA) led to 289 differentially expressed genes (DEGs; 186 upregulated and 103 downregulated) (Fig. S13A). Tissues treated with DA-LBP-GelMA (EA) exhibited 3772 DEGs (1748 upregulated and 2024 downregulated) compared with those treated with DA-LBP-PPEDOT-GelMA (Fig. S13B). Gene Ontology (GO) enrichment analysis categorized the DEGs into biological process (BP), molecular function (MF), and cellular component (CC). The top 20 GO terms included "immune system process" and "response to stimulation" (Fig. 6C), suggesting the involvement of immune regulation in diabetic wound healing under EA combined with conductive microneedles. To identify potential signaling pathways, Kyoto Encyclopedia of Genes and Genomes (KEGG) pathway enrichment analysis was conducted. The results showed that the "Rap1 signaling pathway", "Th17 cell differentiation", and "PI3K-Akt signaling pathway" were among the top 20 enriched pathways (Fig. 6D).

Subsequently, signaling pathway analysis revealed that the combination of EA at GV14 and conductive microneedles enhanced regeneration of wound tissue and peripheral nerves, and had anti-inflammatory and antidepressant effects exerted through modulation of the P38MAPK, PI3K-AKT, and FOXP3 signaling pathways (Fig. 6E and F). The PCR analysis demonstrated that the expression level of P38MAPK in the DA-LBP-PPEDOT-GelMA (EA) group was downregulated compared to the other groups, while the expression levels of PI3K/AKT and FOXP3 were upregulated (Fig. S14). DA-LBP-PPEDOT-GelMA (EA) facilitated cell proliferation and differentiation, and regulation of neuronal development by eliciting activation of the PI3K-Akt signaling pathway [39,40]. Notably, DA-LBP-PPEDOT-GelMA (EA) also elicited upregulation of gene expression associated with nerve growth factor (NGF) and its corresponding receptors compared with the other treatments. This heightened expression induced the activation of the electrosensitive protein Grb2, a pivotal regulator in nerve regeneration [41],

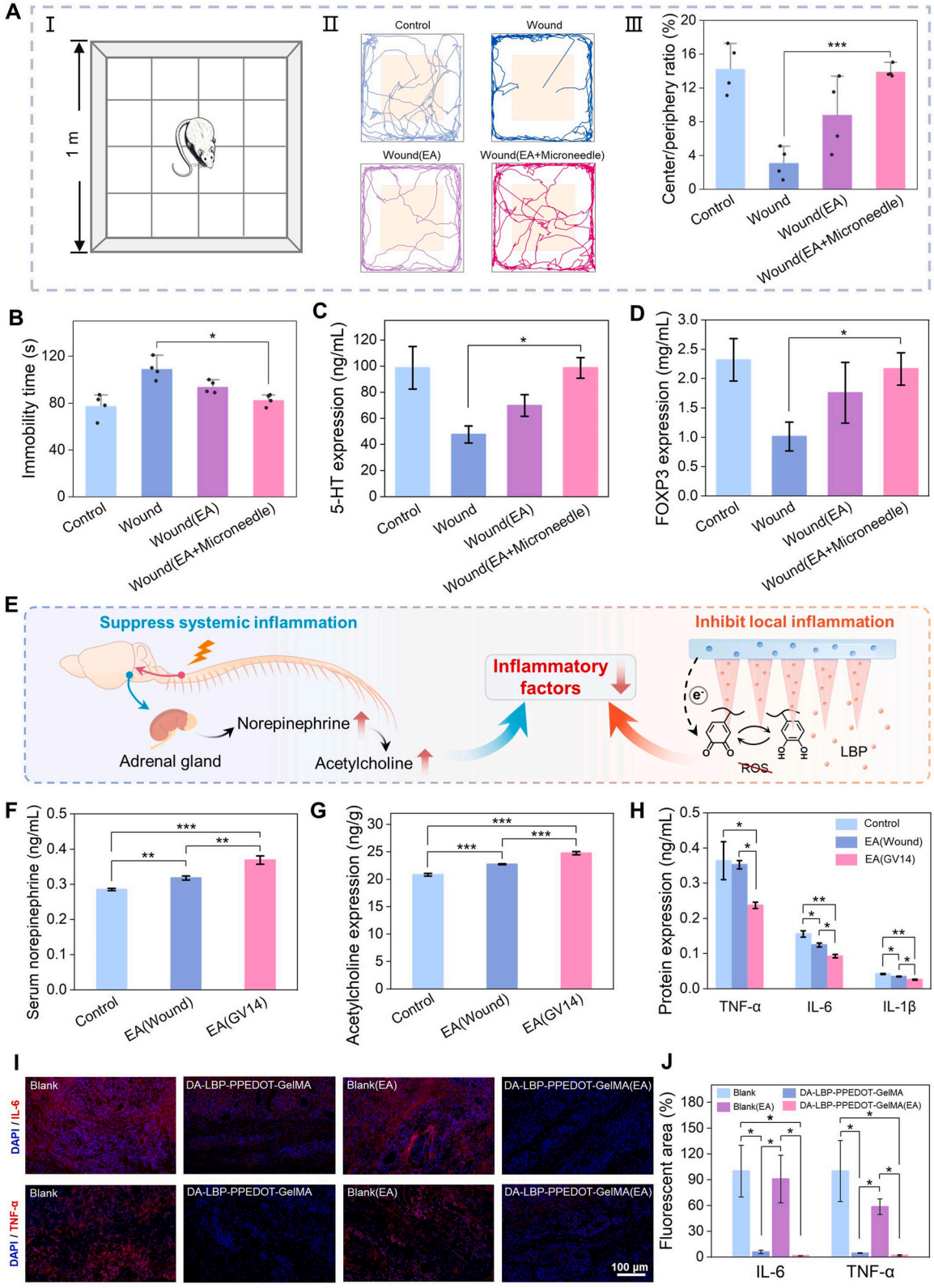

Fig. 5. Alleviation of depressive-like behavior with GV14 electroacupuncture and hydrogel microneedles in SD rats with diabetic wounds. (A) The open field test (OFT): schematic illustration (I); movement trajectories of rats in the four groups (II; groups indicated by the colored bars shown in III); and the ratio of time spent in the central and peripheral zones during the OFT (III). (B) Proportion of time spent struggling (immobility) in the tail suspension test. (C, D) Serum concentrations of 5-HT (C) and FOXP3 (D) in each group. (E) Schematic illustration of the modulation of systemic and local inflammation. (F) Serum concentrations of norepinephrine in each group. (G) Concentrations of acetylcholine in the spleen of each group. (H) Serum concentrations of TNF-α, IL-6 and IL-1β in each group. (I) Representative immunofluorescence staining images of IL-6 and TNF-α at the wound site in each group after 7 days. Blue color (DAPI) indicates nuclei; red color indicates IL-6 and TNF-α. (J) Relative fluorescent area of immunofluorescence staining of IL-6 and TNF-α.

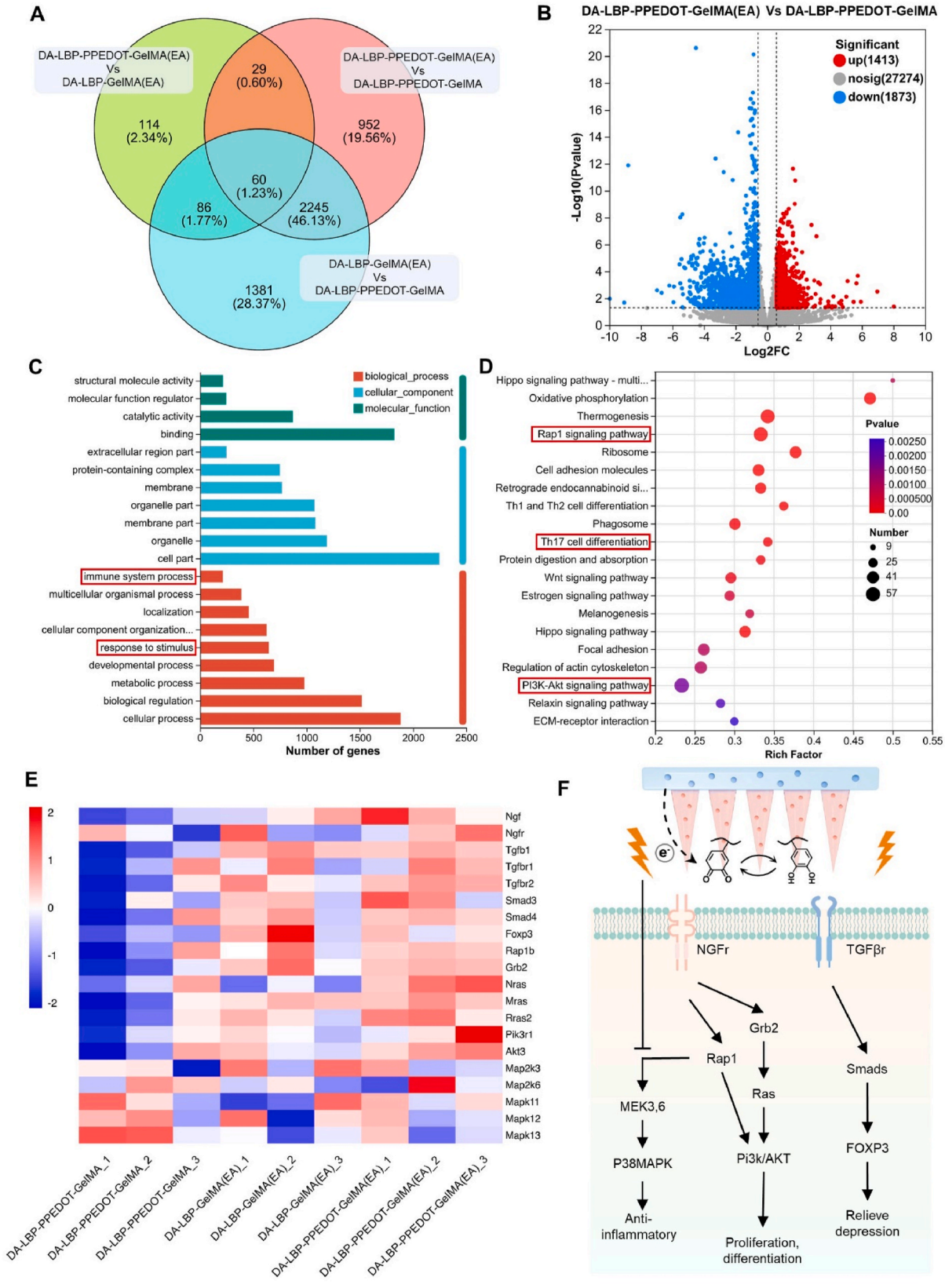

Fig. 6. RNA sequencing analysis of DEGs and regulatory pathways related to EA at GV14 and hydrogel microneedles. (A) Venn diagram illustrating the numbers of DEGs in the various treatment comparisons. (B) Volcano map of differences in gene expression between treatment with DA-LBP-PPEDOT-GelMA (EA) and DA-LBP-PPEDOT-GelMA. (C) GO classification of DEGs in terms of BP, CC, and MF. (D) Enriched KEGG pathways based on differential gene expression. (E) Heatmap analysis of DEGs. (F) Schematic diagram depicting the combined effects of EA at GV14 and hydrogel microneedles on the facilitation of nerve and tissue regeneration surrounding the diabetic wound and alleviation of depressive-like behaviors in rats.

consequently leading to increased reticular activating system (RAS) expression [42]. NGF stimulation is known to prompt Rap1 activation [43], and the concerted actions of RAS and Rap1 synergistically amplify the expression of downstream genes in the PI3K-AKT signaling cascade.

EA at GV14 alone suppressed inflammation by downregulating MEK3/6 and downstream p38 mitogen-activated protein kinase (MAPK)-related gene expression. The combined administration of EA at GV14 and conductive hydrogel microneedles synergistically amplified this regulatory effect. The p38 MAPK cascade plays a pivotal role in inflammatory cytokine synthesis and signaling pathways. Remarkably, inhibiting p38 MAPK has been empirically validated as an effective strategy for attenuating inflammation [44–46].

Treatment with DA-LBP-PPEDOT-GelMA (EA) was also found to mitigate depressive-like behaviors in rats by downregulating FOXP3 levels. The combination of EA at GV14 and conductive hydrogel microneedles led to upregulation of gene expression associated with transforming growth factor β and its receptors. This activation triggers Smad phosphorylation, subsequently resulting in elevated downstream FOXP3 expression levels. FOXP3 serves as an intracellular marker for regulatory T cells [37], with reduced expression levels observed in individuals suffering from depression [47,48].

In summary, comparative analysis between treatment with DA-LBP-PPEDOT-GelMA (EA) and DA-LBP-PPEDOT-GelMA highlighted the promotional effects of EA at GV14 on cell proliferation and differentiation, neuronal development regulation, and depression alleviation. Furthermore, comparison between treatment with DA-LBP-PPEDOT-GelMA (EA) and DA-LBP-GelMA (EA) underscored the synergistic enhancement of these processes through the combination of conductive hydrogel microneedles and EA at GV14.

3.8. Mechanisms of diabetic wound healing through electroacupuncture-assisted hydrogel microneedles

EA effectively activates the vagus–adrenal axis, suppressing systemic inflammation. However, its limitations in precisely modulating local inflammation have restricted its clinical benefit. Most of the currently available hydrogel microneedles lack conductivity, posing challenges in the response to external electrical stimulation, and have limited capacity to regulate prolonged local inflammation. We were able to achieve effective regulation of both local and systemic inflammation through synergistic modulation with conductive hydrogel microneedles and EA at the GV14 acupoint, leading to significant reductions in serum and local levels of TNF-α and IL-6. The effective control of local inflammation, which was characterized by the systemic release of inflammatory mediators and activation of immune cells, prevented the progression to systemic inflammation. Simultaneously, the control of systemic inflammation avoided the exacerbation of local inflammatory reactions caused by the excessive release of pro-inflammatory cytokines resulting from immune overactivation.

EA of GV14 activated the vagus–adrenal axis, effectively suppressing systemic inflammation, but also increased 5-HT levels and ameliorated depressive-like behaviors in rats with diabetic wounds. Furthermore, the coupling of DA in DA-LBP-PPEDOT-GelMA hydrogel microneedles with electrical signals effected long-term regulation of the wound local immune microenvironment via electron transfer-mediated induction of the conversion of DA catechol to DA quinone. Moreover, the conductive microneedles transferred electrical signals that promoted cell migration and collagen deposition. EA of GV14, in conjunction with conductive microneedles, enhanced cell proliferation and differentiation and had anti-inflammatory effects exerted through impacts on the P38MAPK and PI3K-AKT signaling pathways, respectively.

4. Discussion

Persistent and heightened inflammation impedes diabetic wound healing and contributes to depression. Studies show proinflammatory agents like interferon-α used in hepatitis C treatment often leads to depressive symptoms [49–51]. Physical treatments such as EA effectively control inflammation, serving as a strategy to alleviate depression and reduce side effects. EA positively impacts the neuroimmune system, particularly in anti-inflammatory, analgesic, and depressive disorders [52–54]. GV14 is key to bidirectional information transmission, affecting immune system activation and regulation. Clinical studies show that GV14 stimulation improves diabetic peripheral neuropathy [55]. Therefore, EA targeting GV14 alleviates depression by modulating inflammation, benefiting diabetic wound healing.

EA alone lacks the precision to regulate the local wound microenvironment, prompting the design of polyphenol-mediated conductive hydrogel microneedles. Polyphenol modification enhances water dispersibility of PEDOT nanoparticles and facilitates phenol-quinone conversion via electron transfer, allowing the hydrogel microneedles to respond to EA stimulation and continuously scavenge ROS. The hydrogel microneedles demonstrated sufficient strength to penetrate the skin and effectively release LBP in vitro. Additionally, they exhibited excellent cytocompatibility, antioxidant, and immunomodulatory properties, with synergistic electrical stimulation further promoting cell proliferation and spreading.

EA at GV14, combined with polyphenol-mediated conductive hydrogel microneedles, effectively promoted diabetic wound and peripheral nerve repair. This was achieved through the regulation of local and systemic inflammation, significantly reducing serum and local TNF-α and IL-6 levels. The hydrogel microneedles facilitated macrophage polarization from M1 to M2 phenotype, modulating the local immune microenvironment, inhibiting inflammation, and promoting nerve repair. Uncontrolled local inflammation can progress to systemic inflammation, impairing wound healing and causing multi-organ dysfunction. The polyphenol-mediated hydrogel microneedles connect systemic and local inflammation regulation. EA at GV14 inhibits systemic inflammation, while the microneedles provide local electrical stimulation to control local inflammation long-term. This dual regulation fosters an environment conducive to alleviating depression and promoting diabetic wound healing.

Furthermore, this therapeutic strategy upregulated 5-HT and FOXP3 levels, alleviating depressive-like behavior in rats with diabetic wounds, thereby illustrating the link between depression and inflammation. FOXP3, a critical immune regulatory factor in regulatory T cells [56], suppresses the immune response by inhibiting the activation and function of various immune cells [57,58]. Alleviating depression prevented abnormal immune activation and reduced pro-inflammatory cytokine release, thereby mitigating the inflammatory response. Effective inflammation regulation, coupled with depression alleviation, further promoted diabetic wound healing. RNA sequencing revealed the regulation of P38MAPK, PI3K/AKT, and FOXP3 pathways, confirming that this therapeutic strategy disrupts the vicious cycle of inflammation and depression, thereby promoting diabetic wound healing.

5. Conclusion

We developed a strategy that utilizes EA at GV14 together with DA-LBP-PPEDOT-GelMA conductive hydrogel microneedles. This approach effectively suppressed both systemic and local inflammation, establishing a virtuous cycle that facilitated the repair of diabetic wound tissue and peripheral nerves, and alleviated depressive-like behaviors in rats. This strategy of EA combined with polyphenol-mediated anti-inflammatory and antioxidant effects provides a new clinical perspective for clinical diabetic wound management by interrupting the inflammation-depression cycle.

CRediT authorship contribution statement

Yue Hou: Writing – original draft, Visualization, Validation, Software, Methodology, Investigation. **Xiaochuan Guo:** Validation,

Resources, Methodology, Funding acquisition. **Jinhui Ran:** Resources, Methodology, Investigation. **Xiong Lu:** Writing – review & editing, Project administration, Funding acquisition, Conceptualization. **Chaoming Xie:** Writing – review & editing, Supervision, Resources, Funding acquisition, Conceptualization.

Ethics approval and consent to participate

All animal procedures were conducted in accordance with the Guide for the Care and Use of Laboratory Animals of Southwest Jiaotong University, and the experiments were approved by the Animal Ethics Committee of the Laboratory Animal Center of Southwest Jiaotong University (SWJTU-2403-NSFC (076)).

Declaration of competing interest

Authors declare that they have no competing interests.

Acknowledgments

This work was supported by grants from National Key Research and Development Program of China (2023YFC2411300), Guangdong Basic and Applied Basic Research Foundation (2021B1515120019), National Natural Science Foundation of China (32471392, 82072071, 82072073), Fundamental Research Funds for the Central Universities (2682023ZTPY056, 2682024ZTPY003), New Interdisciplinary Cultivation Fund of SWJTU (2682023JX005, 2682022KJ041) and Chengdu Medical Research Project (202317012825). The authors wish to acknowledge the assistance on materials characterization received from Analytical & Testing Center of the Southwest Jiaotong University.

Appendix A. Supplementary data

Supplementary data to this article can be found online at https://doi.org/10.1016/j.bioactmat.2024.11.001.

References

[1] R.T. Crews, B.-J. Shen, L. Campbell, P.J. Lamont, A.J. Boulton, M. Peyrot, R. S. Kirsner, L. Vileikyte, Role and determinants of adherence to off-loading in diabetic foot ulcer healing: a prospective investigation, Diabetes Care 39 (8) (2016) 1371–1377.
[2] T.T. van Sloten, S. Sedaghat, M.R. Carnethon, L.J. Launer, C.D. Stehouwer, Cerebral microvascular complications of type 2 diabetes: stroke, cognitive dysfunction, and depression, Lancet Diabetes Endocrinol. 8 (4) (2020) 325–336.
[3] F. Carr, Diabetes, dopamine and depression, Nat. Rev. Neurosci. 16 (5) (2015) 248, 248.
[4] W.C. Drevets, G.M. Wittenberg, E.T. Bullmore, H.K. Manji, Immune targets for therapeutic development in depression: towards precision medicine, Nat. Rev. Drug Discov. 21 (3) (2022) 224–244.
[5] A.H. Miller, C.L. Raison, The role of inflammation in depression: from evolutionary imperative to modern treatment target, Nat. Rev. Immunol. 16 (1) (2016) 22–34.
[6] F.J. Snoek, M.A. Bremmer, N. Hermanns, Constructs of depression and distress in diabetes: time for an appraisal, Lancet Diabetes Endocrinol. 3 (6) (2015) 450–460.
[7] R.A. Hackett, A. Steptoe, Type 2 diabetes mellitus and psychological stress—a modifiable risk factor, Nat. Rev. Endocrinol. 13 (9) (2017) 547–560.
[8] S.F. Yan, R. Ramasamy, A.M. Schmidt, Mechanisms of disease: advanced glycation end-products and their receptor in inflammation and diabetes complications, Nat. Clin. Pract. Endocrinol. Metabol. 4 (5) (2008) 285–293.
[9] Y. Chen, X. Wang, S. Tao, Q. Wang, P.-Q. Ma, Z.-B. Li, Y.-L. Wu, D.-W. Li, Research advances in smart responsive-hydrogel dressings with potential clinical diabetic wound healing properties, Military Medical Research 10 (1) (2023) 37.
[10] L. Ulloa, S. Quiroz-Gonzalez, R. Torres-Rosas, Nerve stimulation: immunomodulation and control of inflammation, Trends Mol. Med. 23 (12) (2017) 1103–1120.
[11] V.A. Pavlov, K.J. Tracey, Neural regulation of immunity: molecular mechanisms and clinical translation, Nat. Neurosci. 20 (2) (2017) 156–166.
[12] S.-S. Lin, B. Zhou, B.-J. Chen, R.-T. Jiang, B. Li, P. Illes, A. Semyanov, Y. Tang, A. Verkhratsky, Electroacupuncture prevents astrocyte atrophy to alleviate depression, Cell Death Dis. 14 (5) (2023) 343.
[13] Z.J. Zhang, H. Zhao, G.X. Jin, S.C. Man, Y.S. Wang, Y. Wang, H.R. Wang, M.H. Li, L. L. Yam, Z.S. Qin, Assessor-and participant-blinded, randomized controlled trial of dense cranial electroacupuncture stimulation plus body acupuncture for neuropsychiatric sequelae of stroke, Psychiatr. Clin. Neurosci. 74 (3) (2020) 183–190.
[14] S. Liu, Z. Wang, Y. Su, L. Qi, W. Yang, M. Fu, X. Jing, Y. Wang, Q. Ma, A neuroanatomical basis for electroacupuncture to drive the vagal–adrenal axis, Nature 598 (7882) (2021) 641–645.
[15] L. He, Q. Xiao, Y. Zhao, J. Li, S. Reddy, X. Shi, X. Su, K. Chiu, S. Ramakrishna, Engineering an injectable electroactive nanohybrid hydrogel for boosting peripheral nerve growth and myelination in combination with electrical stimulation, ACS Appl. Mater. Interfaces 12 (47) (2020) 53150–53163.
[16] X. Li, W. Yang, H. Xie, J. Wang, L. Zhang, Z. Wang, L. Wang, CNT/sericin conductive nerve guidance conduit promotes functional recovery of transected peripheral nerve injury in a rat model, ACS Appl. Mater. Interfaces 12 (33) (2020) 36860–36872.
[17] X. Wang, S.-h. Shi, H.-j. Yao, Q.-k. Jing, Y.-p. Mo, W. Lv, L.-y. Song, X.-c. Yuan, Z.-g. Li, L.-n. Qin, Electroacupuncture at Dazhui (GV14) and Mingmen (GV4) protects against spinal cord injury: the role of the Wnt/β-catenin signaling pathway, Neural Regeneration Research 11 (12) (2016) 2004.
[18] J. Yan, Y. Ni, L. Tan, S. Zheng, Y. Zhang, J. Liu, Z. Wang, Efficacy and safety of Dazhui (GV 14) as a single acupoint for managing fever: a systematic review, European Journal of Integrative Medicine (2022) 102196.
[19] X. Han, Y. Gao, X. Yin, Z. Zhang, L. Lao, Q. Chen, S. Xu, The mechanism of electroacupuncture for depression on basic research: a systematic review, Chin. Med. 16 (1) (2021) 1–17.
[20] Y. Ye, J. Yu, D. Wen, A.R. Kahkoska, Z. Gu, Polymeric microneedles for transdermal protein delivery, Adv. Drug Deliv. Rev. 127 (2018) 106–118.
[21] Q. Wang, H. Wang, Y. Ma, X. Cao, H. Gao, Effects of electroactive materials on nerve cell behaviors and applications in peripheral nerve repair, Biomater. Sci. (2022).
[22] Z.C. Liu, W.W. Yu, H.C. Zhou, Z.C. Lan, T. Wu, S.M. Xiong, L. Yan, H.B. Liu, Lycium barbarum polysaccharides ameliorate LPS-induced inflammation of RAW264. 7 cells and modify the behavioral score of peritonitis mice, J. Food Biochem. 45 (10) (2021) e13889.
[23] N. Yahfoufi, N. Alsadi, M. Jambi, C. Matar, The immunomodulatory and anti-inflammatory role of polyphenols, Nutrients 10 (11) (2018) 1618.
[24] Z. Jia, X. Lv, Y. Hou, K. Wang, F. Ren, D. Xu, Q. Wang, K. Fan, C. Xie, X. Lu, Mussel-inspired nanozyme catalyzed conductive and self-setting hydrogel for adhesive and antibacterial bioelectronics, Bioact. Mater. 6 (9) (2021) 2676–2687.
[25] T. Zhou, L. Yan, C. Xie, P. Li, L. Jiang, J. Fang, C. Zhao, F. Ren, K. Wang, Y. Wang, A mussel-inspired persistent ROS-scavenging, electroactive, and osteoinductive scaffold based on electrochemical-driven in situ nanoassembly, Small 15 (25) (2019) 1805440.
[26] Z. Du, F. Qiao, L. Tong, W. Zhang, X. Mou, X. Zhao, M.F. Maitz, H. Wang, N. Huang, Z. Yang, Mimicking Mytilus edulis foot protein: a versatile strategy for robust biomedical coatings, Innovation 5 (5) (2024).
[27] R.A. Zangmeister, T.A. Morris, M.J. Tarlov, Characterization of polydopamine thin films deposited at short times by autoxidation of dopamine, Langmuir 29 (27) (2013) 8619–8628.
[28] X. Zhou, H. Cui, M. Nowicki, S. Miao, S.-J. Lee, F. Masood, B.T. Harris, L.G. Zhang, Three-dimensional-bioprinted dopamine-based matrix for promoting neural regeneration, ACS Appl. Mater. Interfaces 10 (10) (2018) 8993–9001.
[29] S.P. Sullivan, D.G. Koutsonanos, M. del Pilar Martin, J.W. Lee, V. Zarnitsyn, S.-O. Choi, N. Murthy, R.W. Compans, I. Skountzou, M.R. Prausnitz, Dissolving polymer microneedle patches for influenza vaccination, Nat. Med. 16 (8) (2010) 915–920.
[30] L. Guan, X. Ou, Z. Wang, X. Li, Y. Feng, X. Yang, W. Qu, B. Yang, Q. Lin, Electrical stimulation-based conductive hydrogel for immunoregulation, neuroregeneration and rapid angiogenesis in diabetic wound repair, Sci. China Mater. 66 (3) (2023) 1237–1248.
[31] A.D. Gaudet, P.G. Popovich, M.S. Ramer, Wallerian degeneration: gaining perspective on inflammatory events after peripheral nerve injury, J. Neuroinflammation 8 (2011) 1–13.
[32] P. Liu, J. Peng, G.-H. Han, X. Ding, S. Wei, G. Gao, K. Huang, F. Chang, Y. Wang, Role of macrophages in peripheral nerve injury and repair, Neural regeneration research 14 (8) (2019) 1335–1342.
[33] N. Mokarram, A. Merchant, V. Mukhatyar, G. Patel, R.V. Bellamkonda, Effect of modulating macrophage phenotype on peripheral nerve repair, Biomaterials 33 (34) (2012) 8793–8801.
[34] P. Blier, N.M. Ward, Is there a role for 5-HT1A agonists in the treatment of depression? Biol. Psychiatr. 53 (3) (2003) 193–203.
[35] C.N. Yohn, M.M. Gergues, B.A. Samuels, The role of 5-HT receptors in depression, Mol. Brain 10 (2017) 1–12.
[36] C.M. Nguyen, D.M. Tartar, M.D. Bagood, M. So, A.V. Nguyen, A. Gallegos, D. Fregoso, J. Serrano, D. Nguyen, D. Degovics, Topical fluoxetine as a novel therapeutic that improves wound healing in diabetic mice, Diabetes 68 (7) (2019) 1499–1507.
[37] Y. Li, B. Xiao, W. Qiu, L. Yang, B. Hu, X. Tian, H. Yang, Altered expression of CD4+ CD25+ regulatory T cells and its 5-HT1a receptor in patients with major depression disorder, J. Affect. Disord. 124 (1–2) (2010) 68–75.
[38] B. Devlin, J.R. Kelsoe, P. Sklar, M.J. Daly, M.C. O'Donovan, N. Craddock, K. S. Kendler, L. A Weiss, N.R. Wray, Psychiatric genome-wide association study analyses implicate neuronal, immune and histone pathways, Nat. Neurosci. 18 (2) (2015) 199–209.
[39] J. Zhong, RAS and downstream RAF-MEK and PI3K-AKT signaling in neuronal development, function and dysfunction, Biol. Chem. 397 (3) (2016) 215–222.

[40] M. Zhao, B. Song, J. Pu, T. Wada, B. Reid, G. Tai, F. Wang, A. Guo, P. Walczysko, Y. Gu, Electrical signals control wound healing through phosphatidylinositol-3-OH kinase-γ and PTEN, Nature 442 (7101) (2006) 457–460.
[41] R. Mao, B. Yu, J. Cui, Z. Wang, X. Huang, H. Yu, K. Lin, S.G. Shen, Piezoelectric stimulation from electrospun composite nanofibers for rapid peripheral nerve regeneration, Nano Energy 98 (2022) 107322.
[42] T. Takenawa, H. Miki, K. Matuoka, Signaling through Grb2/Ash-control of the Ras pathway and cytoskeleton. Protein Modules in Signal Transduction, 1998, pp. 325–342.
[43] C. Wu, C.-F. Lai, W.C. Mobley, Nerve growth factor activates persistent Rap1 signaling in endosomes, J. Neurosci. 21 (15) (2001) 5406–5416.
[44] J.-Q. Fang, J.-Y. Du, Y. Liang, J.-F. Fang, Intervention of electroacupuncture on spinal p38 MAPK/ATF-2/VR-1 pathway in treating inflammatory pain induced by CFA in rats, Mol. Pain 9 (2013) 1744–8069, 9-13.
[45] S. Kumar, J. Boehm, J.C. Lee, p38 MAP kinases: key signalling molecules as therapeutic targets for inflammatory diseases, Nat. Rev. Drug Discov. 2 (9) (2003) 717–726.
[46] K.M.K. Rao, MAP kinase activation in macrophages, J. Leukoc. Biol. 69 (1) (2001) 3–10.
[47] E.-J. Yang, M.A. Rahim, E. Griggs, R. Iban-Arias, G.M. Pasinetti, Transient anxiety- and depression-like behaviors are linked to the depletion of Foxp3-expressing cells via inflammasome in the brain, PNAS nexus 2 (8) (2023) pgad251.
[48] T.T. Le, J. Savitz, H. Suzuki, M. Misaki, T.K. Teague, B.C. White, J.H. Marino, G. Wiley, P.M. Gaffney, W.C. Drevets, Identification and replication of RNA-Seq gene network modules associated with depression severity, Transl. Psychiatry 8 (1) (2018) 180.
[49] S. Bonaccorso, V. Marino, M. Biondi, F. Grimaldi, F. Ippoliti, M. Maes, Depression induced by treatment with interferon-alpha in patients affected by hepatitis C virus, J. Affect. Disord. 72 (3) (2002) 237–241.
[50] A. Reichenberg, J.M. Gorman, D.T. Dieterich, Interferon-induced depression and cognitive impairment in hepatitis C virus patients: a 72 week prospective study, Aids 19 (2005) S174–S178.
[51] J.C. Felger, E. Haroon, B.J. Woolwine, C.L. Raison, A.H. Miller, Interferon-alpha-induced inflammation is associated with reduced glucocorticoid negative feedback sensitivity and depression in patients with hepatitis C virus, Physiol. Behav. 166 (2016) 14–21.
[52] J.-Y. Park, U. Namgung, Electroacupuncture therapy in inflammation regulation: current perspectives, J. Inflamm. Res. (2018) 227–237.
[53] H. Jiang, S. Deng, J. Zhang, J. Chen, B. Li, W. Zhu, M. Zhang, C. Zhang, Z. Meng, Acupuncture treatment for post-stroke depression: intestinal microbiota and its role, Front. Neurosci. 17 (2023) 1146946.
[54] B. Dou, Y. Li, J. Ma, Z. Xu, W. Fan, L. Tian, Z. Chen, N. Li, Y. Gong, Z. Lyu, Role of neuroimmune crosstalk in mediating the anti-inflammatory and analgesic effects of acupuncture on inflammatory pain, Front. Neurosci. 15 (2021) 695670.
[55] W. Yao-chi, W. Huan-gan, Research progress of acupuncture and moxibustion in treating diabetes mellitus, Journal of Acupuncture and Tuina Science 3 (2005) 50–54.
[56] L. Lu, J. Barbi, F. Pan, The regulation of immune tolerance by FOXP3, Nat. Rev. Immunol. 17 (11) (2017) 703–717.
[57] A.Y. Rudensky, Regulatory T cells and Foxp3, Immunol. Rev. 241 (1) (2011) 260–268.
[58] J.-H. Tao, M. Cheng, J.-P. Tang, Q. Liu, F. Pan, X.-P. Li, Foxp3, regulatory T cell, and autoimmune diseases, Inflammation 40 (2017) 328–339.